$pp \to ppK^+K^-$ reaction at high energies

P. Lebiedowicz[1,*] and A. Szczurek[1,2,†]

[1]*Institute of Nuclear Physics PAN, PL-31-342 Cracow, Poland*
[2]*University of Rzeszów, PL-35-959 Rzeszów, Poland*
(Received 11 November 2011; published 25 January 2012)

We evaluate differential distributions for the four-body $pp \to ppK^+K^-$ reaction at high energies, which constitutes an irreducible background to three-body processes $pp \to ppM$, where $M = \phi, f_2(1275), f_0(1500), f_2'(1525), \chi_{c0}$. We consider the central diffractive contribution mediated by Pomeron and Reggeon exchanges as well as a completely new mechanism of emission of kaons from the proton lines. We include absorption effects due to proton-proton interaction and kaon-kaon rescattering. We compare our results with measured cross sections for the CERN Intersecting Storage Rings experiment. We make predictions for future experiments at RHIC, Tevatron, and LHC. Differential distributions in invariant two-kaon mass, kaon rapidities, and transverse momenta of kaons are presented. Two-dimensional distribution in (y_{K^+}, y_{K^-}) is particularly interesting. The higher the incident energy, the higher preference for the same-hemisphere emission of kaons. We find that the kaons from the new mechanism of emission directly from proton lines are produced rather forward and backward but the corresponding cross section is rather small. The processes considered here constitute a sizeable contribution to the total proton-proton cross section as well as to the kaon inclusive cross section. We consider a measurement of exclusive production of a scalar χ_{c0} meson in the proton-proton collisions via $\chi_{c0} \to K^+K^-$ decay. The corresponding amplitude for exclusive central diffractive χ_{c0} meson production is calculated within the k_t-factorization approach. The influence of kinematical cuts on the signal-to-background ratio is discussed.

I. INTRODUCTION

The exclusive $pp \to ppK^+K^-$ reaction was studied only at low energy [1,2]. Here the dominant mechanisms are exclusive $a_0(980)$ and $f_0(980)$ production [1] or excitation of the nucleon and Λ resonances [2]. The main aim of this paper is to discuss mechanisms of exclusive K^+K^- production in hadron-hadron collisions at high energies. Processes of central exclusive production became recently a very active field of research (see, e.g., Ref. [3] and references therein). Although the attention is paid mainly to high-p_t processes that can be used for new physics searches (exclusive Higgs, $\gamma\gamma$ interactions, etc.), measurements of low-p_t signals are also very important as they can help to constrain models of the backgrounds for the former ones. The $pp \to ppK^+K^-$ reaction is a natural background for exclusive production of resonances decaying into K^+K^- channel, such as: $\phi, f_2(1270), f_0(1500), f_2'(1525), \chi_{c0}$. The expected nonresonant background can be modeled using a "nonperturbative" framework, mediated by Pomeron-Pomeron fusion with an intermediate off-shell pion/kaon exchanged between the final-state particles. The two-pion background to exclusive production of $f_0(1500)$ meson was discussed in Ref. [4]. In Refs. [5,6], we have studied the production of $\pi^+\pi^-$ pairs for low

and high energies. Here we wish to present a similar analysis for K^+K^- production at high energies. The dominant mechanism of the $pp \to pp\pi^+\pi^-$, $pp \to ppK^+K^-$ reactions at high energies is relatively simple compared to that of the $pp \to nn\pi^+\pi^+$ [7] or $pp \to pp\pi^0\pi^0$ processes. In Ref. [8] a possible measurement of the exclusive $\pi^+\pi^-$ production at the LHC with tagged forward protons has been studied.

A study of the centrally produced $\pi^+\pi^-$ and K^+K^- channels in pp collisions has been performed experimentally at an incident-beam momenta of 300 GeV/c ($\sqrt{s} = 23.8$ GeV) [9] and 450 GeV/c ($\sqrt{s} = 29.1$ GeV) [10]. In the latter paper, a study has been performed of the resonance production rate as a function of the difference in the transverse momentum vectors (dP_T) between the particles exchanged from vertices. An analysis of the dP_T dependence of the four-momentum transfer behavior shows that the $\rho^0(770)$, $\phi(1020)$, $f_2(1270)$, and $f_2'(1525)$ are suppressed at small dP_T in contrast to the $f_0(980)$, $f_0(1500)$, and $f_0(1710)$. Different distributions are observed in the azimuthal angle (defined as the angle between the p_t vectors of the two outgoing protons) for the different resonances (see [10]). The mass spectrum of the exclusive K^+K^- system at the CERN Intersecting Storage Rings (ISR) is shown, e.g., in Ref. [11] at $\sqrt{s} = 63$ GeV and in Ref. [12] at $\sqrt{s} = 62$ GeV (this is the highest energy at which normalized experimental data exist).

Recently, there was interest in central exclusive production of P-wave quarkonia (see Refs. [13–17]) where the

*piotr.lebiedowicz@ifj.edu.pl
†antoni.szczurek@ifj.edu.pl

QCD mechanism is similar to the exclusive production of the Higgs boson. Furthermore, the $\chi_{c(0,2)}$ states are expected to annihilate via two-gluon processes into light mesons, in particular, into K^+K^-. Also some glueball candidates [18] can be searched for in this channel.

The cross section for central exclusive production of χ_c mesons has been measured recently in proton-antiproton collisions at the Tevatron [19]. In this experiment χ_c mesons are identified via decay to the $J/\psi + \gamma$ with the $J/\psi \to \mu^+\mu^-$ channel. At the Tevatron, the experimental invariant mass resolution was not sufficient to distinguish between scalar, axial, and tensor χ_c. While the branching fractions to this channel for axial and tensor mesons are large [20] [$\mathcal{B} = (34.4 \pm 1.5)\%$ and $\mathcal{B} = (19.5 \pm 0.8)\%$, respectively] the branching fraction for the scalar meson is very small $\mathcal{B} = (1.16 \pm 0.08)\%$ [20]. Theoretical calculations have shown [15] that the cross section for exclusive χ_{c0} production obtained within the k_t factorization is much bigger than that for χ_{c1} and χ_{c2}. As a consequence, all χ_c mesons give similar contributions to the $J/\psi + \gamma$ decay channel. Clearly, the measurement via decay to the $J/\psi + \gamma$ channel at Tevatron cannot provide a cross section for different species of χ_c.

The scalar χ_{c0} meson decays into several two-body (e.g., $\pi\pi$, K^+K^-, $p\bar{p}$) and four-body final states (e.g., $\pi^+\pi^-\pi^+\pi^-$, $\pi^+\pi^-K^+K^-$). The observation of χ_{c0} central exclusive production via two-body decay channels is of special interest for studying the dynamics of heavy quarkonia. The measurement of exclusive production of the χ_{c0} meson in proton-(anti)proton collisions via $\chi_{c0} \to \pi^+\pi^-$ decay has been already discussed in Ref. [21]. In the present paper, we analyze a possibility to measure χ_{c0} via its decay to the K^+K^- channel. The branching fraction to this channel is relatively large $\mathcal{B}(\chi_{c0} \to K^+K^-) = (0.61 \pm 0.035)\%$ [20]. In addition, the axial χ_{c1} does not decay to the KK channel and the branching ratio for the χ_{c2} decay into two kaons is smaller $\mathcal{B}(\chi_{c2} \to K^+K^-) = (0.109 \pm 0.008)\%$ [20]. A much smaller cross section for χ_{c2} production as obtained from theoretical calculation means that only χ_{c0} will contribute to the signal.

Exclusive charmonium decays can be also studied in e^+e^- colliders. Here the χ_{cJ} states are copiously produced in the radiative decays $\psi(2S) \to \gamma\chi_{cJ}$ [20]. Recently, the BESIII Collaboration performed a measurement of the hadronic decays of the three χ_{cJ} states to $p\bar{p}K^+K^-$

$[\bar{p}K^+\Lambda(1520)$, $\Lambda(1520)\bar{\Lambda}(1520)$, and $\phi p\bar{p}]$ [22]. In the present paper, we discuss a possibility to measure χ_{c0} in the K^+K^- channel. Here, continuum backgrounds are expected to be larger than in the e^+e^- collisions. This will discussed in the present paper.

II. CENTRAL DIFFRACTIVE CONTRIBUTION

A. The KN scattering

In order to fix the parameters of our double Pomeron (IP) exchange (DPE) model we consider first elastic KN scattering. The forward amplitudes $M_{KN}(s, t = 0)$ of the elastic scatterings are written in terms of the Regge exchanges:

$$M_{K^\pm p \to K^\pm p}(s, 0) = A_{IP}(s, 0) + A_{f_2}(s, 0) + A_{a_2}(s, 0)$$
$$\mp A_\omega(s, 0) \mp A_\rho(s, 0),$$
$$M_{K^\pm n \to K^\pm n}(s, 0) = A_{IP}(s, 0) + A_{f_2}(s, 0) - A_{a_2}(s, 0)$$
$$\mp A_\omega(s, 0) \pm A_\rho(s, 0). \quad (2.1)$$

The optical theorem relates the total cross section for the scattering of a pair of hadrons to the amplitude for elastic scattering: $\mathrm{Im}M_{el}(s, t = 0) \sim s\sigma_{\mathrm{tot}}(s)$. When the center-of-mass energy $\sqrt{s}$ is large, the elastic KN scattering amplitude is a sum of the terms:

$$A_i(s, t) = \eta_i s C_i^{KN} \left(\frac{s}{s_0}\right)^{\alpha_i(t)-1} \exp\left(\frac{B_{KN}^i}{2}t\right), \quad (2.2)$$

where $i = IP$, f_2, a_2, ω, and ρ. The energy scale s_0 is fixed at $s_0 = 1$ GeV^2. The values of coupling constants (C_i^{KN}) are taken from the Donnachie-Landshoff analysis of the total cross section in several hadronic reactions [23]. The parameters of Regge linear trajectories [$\alpha_i(t) = \alpha_i(0) + \alpha_i't$] and signature factors (η_i) used in the present calculations are listed in Table I. The slope of the elastic KN scattering can be written as

$$B(s) = B_{KN}^i + 2\alpha_i' \ln\left(\frac{s}{s_0}\right), \quad (2.3)$$

and only the B_{KN}^i parameters are adjusted to the existing experimental data for the elastic KN scattering.

The differential elastic cross section is expressed with the help of the elastic scattering amplitude, usually as

TABLE I. Parameters of Pomeron and Reggeon exchanges determined from elastic and total cross sections used in the present calculations.

i	η_i	$\alpha_i(t)$	C_i^{NN} (mb)	C_i^{KN} (mb)	C_i^{KK} (mb)
IP	i	$1.0808 + (0.25$ GeV$^{-2})t$	21.7	11.82	$\simeq 6.438$
f_2	$-0.860\,895 + i$	$0.5475 + (0.93$ GeV^{-2}t	75.4875	15.67	$\simeq 3.253$
ρ	$-1.161\,58 - i$	$0.5475 + (0.93$ GeV^{-2}t	1.0925	2.05	$\simeq 3.847$
a_2	$-0.860\,895 + i$	$0.5475 + (0.93$ GeV^{-2}t	1.7475	1.585	$\simeq 1.438$
ω	$-1.161\,58 - i$	$0.5475 + (0.93$ GeV^{-2}t	20.0625	7.055	$\simeq 2.481$

$$\frac{d\sigma_{el}}{dt} = \frac{1}{16\pi s^2}|M_{KN}(s,t)|^2. \quad (2.4)$$

The differential distributions $d\sigma_{el}/dt$ for both K^+p and K^-p elastic scattering for three incident-beam momenta of $P_{lab} = 5$ GeV, $P_{lab} = 50$ GeV, and $P_{lab} = 200$ GeV are shown in Fig. 1. With the slope parameters, as in Ref. [6], $B_{IP}^{KN} = B_{IP}^{\pi N} = 5.5$ GeV^{-2}, $B_{IR}^{KN} = B_{IR}^{\pi N} = 4$ GeV^{-2} for Pomeron and Reggeon (IR) exchanges; a rather good description of experimental $d\sigma_{el}/dt$ is achieved. The exception is the low energy K^+p scattering. Here, Λ baryon exchange is a possible mechanism in addition to Pomeron and Reggeon exchanges.

We describe the existing experimental data for elastic K^-p and K^-n scattering for $\sqrt{s} > 3$ GeV and for elastic K^+p scattering for $\sqrt{s} > 7$ GeV as can be seen from Fig. 2. As will be discussed in the course of this paper, the small Kp energies where we fail to describe the experimental data are important only at large (pseudo)rapidities of K^+ or K^- where a measurement is practically impossible. In the Regge approach, the high-energy cross section is dominated by the Pomeron exchange (dashed lines). The Reggeon exchanges dominate in the resonance region (dash-dotted lines). While the total cross section is just a sum of the Pomeron and Reggeon terms, the elastic cross section has the interference term (long-dashed lines). In
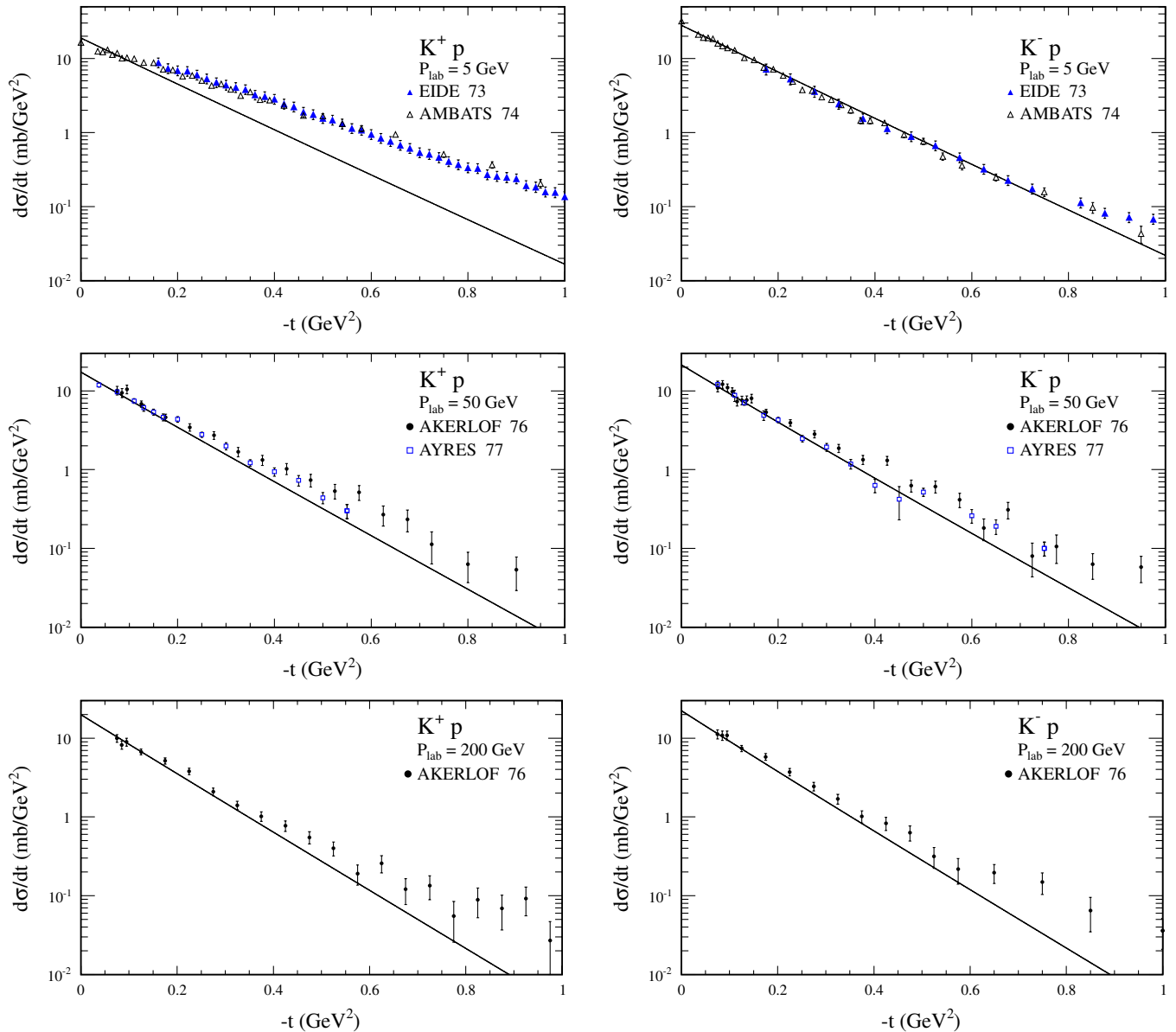
FIG. 1 (color online).   Differential distributions for K^+p (left) and K^-p (right) elastic scattering for three incident-beam momenta of $P_{lab} = 5, 50, 200$ GeV. The experimental data are taken from Refs. [32] and the names of first authors are given explicitly in the figure.
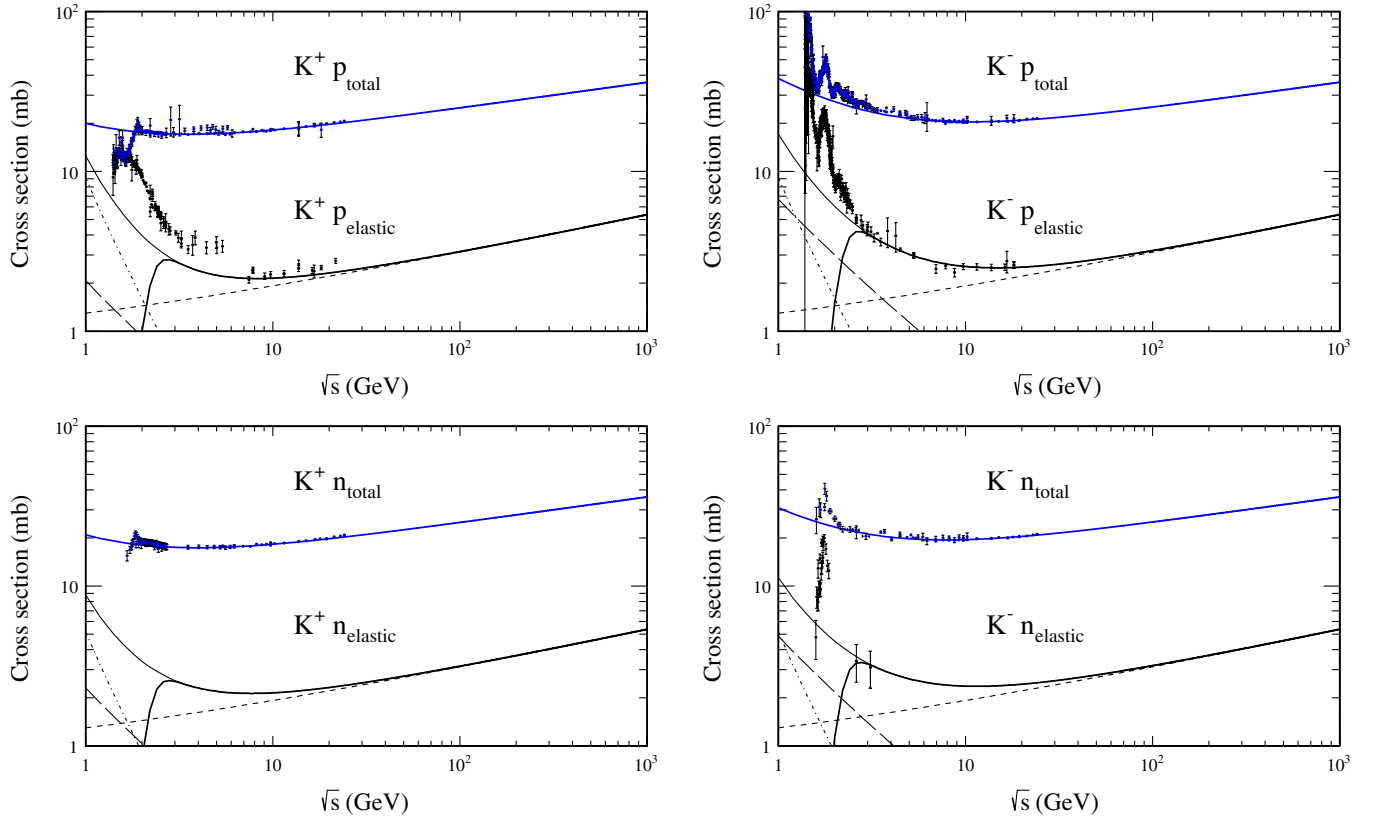
FIG. 2 (color online). The integrated cross section for the KN total and elastic scattering. The experimental data are taken from particle data book [20]. The lines are explained in the main text.

order to exclude low energy regions, the $M_{KN}(s, t)$ elastic scattering amplitudes are corrected by purely pheno-menological smooth cutoff correction factor (as in Ref. [6]).

Our model sufficiently well describes the KN data and includes absorption effects due to kaon-nucleon rescatter-ings in an effective way. This has a clear advantage for applications to the $pp \to ppK^+K^-$ reaction where the KN absorption effects do not need to be included explicitly. Having fixed the parameters we can proceed to our four-body $pp \to ppK^+K^-$ reaction.

B. Central diffractive production of K^+K^-

The dominant mechanism of the exclusive production of K^+K^- pairs at high energies is sketched in Fig. 3. The formalism used in the calculation of the amplitude is explained in detail elsewhere for the $\pi^+\pi^-$ production [6,21] and here only main aspects are discussed. The full amplitude for the process $pp \to pK^+K^-p$ (with four-momenta $p_a + p_b \to p_1 + p_3 + p_4 + p_2$, respectively) is a sum of the Born and rescattering amplitudes

$$\mathcal{M}_{pp\to ppKK}^{\text{full}} = \mathcal{M}^{\text{Born}} + \mathcal{M}^{pp-\text{rescatt}} + \mathcal{M}^{KK-\text{rescatt}}. \quad (2.5)$$
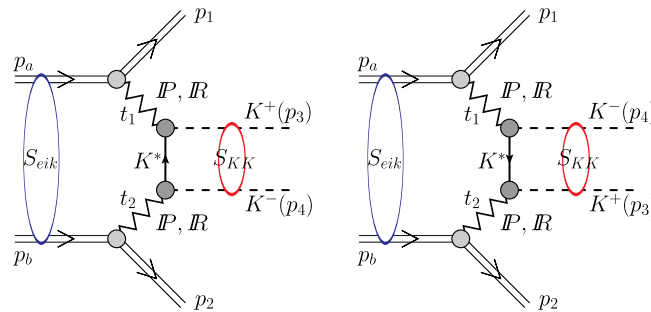
FIG. 3 (color online). The central diffractive mechanism of exclusive production of K^+K^- pairs including the absorptive corrections due to proton-proton interactions as well as kaon-kaon rescattering. S_{eik} (S matrix for eikonal approach).

The Born amplitude can be written as

$$\mathcal{M}^{\text{Born}} = M_{13}(s_{13}, t_1)F_K(\hat{t})\frac{1}{\hat{t} - m_K^2}F_K(\hat{t})M_{24}(s_{24}, t_2)$$
$$+ M_{14}(s_{14}, t_1)F_K(\hat{u})\frac{1}{\hat{u} - m_K^2}F_K(\hat{u})M_{23}(s_{23}, t_2), \tag{2.6}$$

where $M_{ik}(s_{ik}, t_i)$ denotes "interaction" between the forward proton ($i = 1$) or backward proton ($i = 2$) and one of the two kaons ($k = 3$ for K^+, $k = 4$ for K^-). The energy dependence of the KN elastic amplitudes is parametrized in terms of Pomeron and f_2, a_2, ω, and ρ Reggeon exchanges as explained in Sec. II A. The Donnachie-Landshoff parametrization is used only above resonance regions for the KN subsystem energy $\sqrt{s_{ik}} > 2 - 3$ GeV. In order to exclude resonance regions, the M_{ik} terms are corrected by purely phenomenological smooth cutoff correction factors which, in practice, modify the cross section only at large rapidities [6].

The kaon exchange as a meson exchange is a correct description at rather low energies. At higher energies a kaon Reggezation is required [21]. This is done by the following replacement:

$$\frac{1}{\hat{t}/\hat{u} - m_K^2} \to \beta_M(\hat{s})\frac{1}{\hat{t}/\hat{u} - m_K^2} + \beta_R(\hat{s})\mathcal{P}^K(\hat{t}/\hat{u}, \hat{s}), \quad (2.7)$$

where we have introduced the kaon Regge propagator $\mathcal{P}^K(\hat{t}/\hat{u}, \hat{s}) = \mathcal{P}^\pi(\hat{t}/\hat{u}, \hat{s})$ (see Ref. [21,24]). Above we have written $\hat{s}, \hat{t}, \hat{u}$ to stress that these are quantities for a subprocess rather than for a full reaction. $\beta_M(\hat{s})$ and $\beta_R(\hat{s})$ are the phenomenological functions whose role is to interpolate between the meson and the Reggeon exchange. Here, as in Ref. [21], we parametrize them as $\beta_M(\hat{s}) = \exp(-(\hat{s} - 4m_K^2)/\Lambda_{int}^2)$, $\beta_R(\hat{s}) = 1 - \beta_M(\hat{s})$. The parameter Λ_{int} can be fitted to experimental data. From our general experience in hadronic physics, we expect it to be about $\Lambda_{int} \sim 1$–2 GeV.

The form factors, $F(\hat{t}/\hat{u})$, correct for the off-shellness of the intermediate kaons in the middle of the diagrams shown in Fig. 3. In the following they are parametrized as

$$F_K(\hat{t}/\hat{u}) = \exp\left(\frac{\hat{t}/\hat{u} - m_K^2}{\Lambda_{\text{off}}^2}\right), \tag{2.8}$$

where the parameter Λ_{off} is not known in general but, in principle, could be fitted to the normalized experimental data. How to extract Λ_{off} will be discussed in the results section.

The absorptive corrections to the Born amplitude due to pp interactions were taken into account in [21] as

$$\mathcal{M}^{pp-\text{rescatt.}} = \frac{i}{8\pi^2 s}\int d^2\boldsymbol{k}_t A_{pp\to pp}^{I\!P}(s, k_t^2)$$
$$\times \mathcal{M}^{\text{Born}}(\boldsymbol{p}_{a,t}^* - \boldsymbol{p}_{1,t}, \boldsymbol{p}_{b,t}^* - \boldsymbol{p}_{2,t}), \tag{2.9}$$

where $p_a^* = p_a - k_t$, $p_b^* = p_b + k_t$, and k_t is the transverse momentum exchanged in the blob.

The formulas presented so far do not include $\pi\pi, KK \to KK$ rescatterings. The pion-pion interaction at high energies was studied, e.g., in Refs. [25,26]. In full analogy to those works at the higher energies, one can include the $\pi\pi, KK \to KK$ rescattering for our four-body reaction by replacing the normal (or Reggeized) pion/kaon propagators (including vertex form factors).

The $KK \to KK$ subprocess amplitude for t and u diagrams in Fig. 3 is written in the high-energy approximation

$$\frac{F_K^2(\hat{t})}{\hat{t} - m_K^2} \to \frac{i}{16\pi^2\hat{s}}\int d^2\kappa \frac{F_K^2(\hat{t}_1)}{\hat{t}_1 - m_K^2}M_{K^+K^-\to K^+K^-}(\hat{s}, \hat{t}_2),$$
$$\frac{F_K^2(\hat{u})}{\hat{u} - m_K^2} \to \frac{i}{16\pi^2\hat{s}}\int d^2\kappa \frac{F_K^2(\hat{u}_1)}{\hat{u}_1 - m_K^2}M_{K^-K^+\to K^-K^+}(\hat{s}, \hat{u}_2). \tag{2.10}$$

Here the integration is over the momentum in the loop (see [26]). The quantities $\hat{t}_1, \hat{u}_1$ and $\hat{t}_2, \hat{u}_2$ are four-momenta squared of the exchanged objects in the first and in the second step of the rescattering process. Other details are explained in [25].

The elastic amplitudes in the $KK \to KK$ subprocesses are written as

$$M_{KK\to KK}(\hat{s}, \hat{t}_2/\hat{u}_2) = \beta_M'(\hat{s})A_{KK\to KK}^{V-\text{exch.}}(\hat{t}_2/\hat{u}_2)$$
$$+ \beta_R'(\hat{s})A_{KK\to KK}^{\text{Regge}}(\hat{s}, \hat{t}_2/\hat{u}_2), \quad (2.11)$$

for vector meson ($V = \rho, \omega, \phi$) exchanges and $\beta_M'(\hat{s}) = \exp(-(\hat{s} - 4m_K^2)/\Delta\hat{s})$, $\beta_R'(\hat{s}) = 1 - \beta_M'(\hat{s})$, $\Delta\hat{s} = 9$ GeV^2.

The Regge-type interaction which includes Pomeron and Reggeon (f_2, a_2, ρ, and ω) exchanges applies at higher energies:

$$A_{K^+K^-\to K^+K^-}^{\text{Regge}}(\hat{s}, \hat{t}_2) = \eta_i\hat{s}C_i^{KK}\left(\frac{\hat{s}}{\hat{s}_0}\right)^{\alpha_i(\hat{t}_2)-1}\exp\left(\frac{B_{KK}^i}{2}\hat{t}_2\right),$$
$$A_{K^-K^+\to K^-K^+}^{\text{Regge}}(\hat{s}, \hat{u}_2) = \eta_i\hat{s}C_i^{KK}\left(\frac{\hat{s}}{\hat{s}_0}\right)^{\alpha_i(\hat{u}_2)-1}\exp\left(\frac{B_{KK}^i}{2}\hat{u}_2\right), \tag{2.12}$$

where the scale parameter $\hat{s}_0$ is taken as 1 GeV^2 and the C_i^{KK} coupling constants can be evaluated assuming Regge factorization $C_i^{KK} = (C_i^{KN})^2/C_i^{NN}$ and are listed in Table I.

At low energies, the Regge-type of interactions are not realistic and rather $V = \rho, \omega, \phi$ meson exchanges must be taken into account:

$A^{V-\text{exch}}_{K^+K^-\to K^+K^-}(\hat{t}_2)$

$= g_{KKV}F_{KKV}(\hat{t}_2)\dfrac{(p_3^{*\mu}+p_3^\mu)P_{\mu\nu}(p_4^{*\nu}+p_4^\nu)}{\hat{t}_2-m_V^2+im_V\Gamma_V}g_{KKV}F_{KKV}(\hat{t}_2),$

$A^{V-\text{exch}}_{K^-K^+\to K^-K^+}(\hat{u}_2)$

$= g_{KKV}F_{KKV}(\hat{u}_2)\dfrac{(p_3^{*\mu}+p_4^\mu)P_{\mu\nu}(p_4^{*\nu}+p_3^\nu)}{\hat{u}_2-m_V^2+im_V\Gamma_V}g_{KKV}F_{KKV}(\hat{u}_2),$

$$(2.13)$$

where $P_{\mu\nu}(k)=-g_{\mu\nu}+k_\mu k_\nu/m_V^2$ and the KKV coupling constants g_{KKV} are given from SU(3) symmetry relations $2g_{KK\omega}=\sqrt{2}g_{KK\phi}=2g_{KK\rho}=g_{\rho\pi\pi}=6.04$ [27], where the value of $g_{\rho\pi\pi}$ is determined by the decay width of the ρ meson.

Again the $\pi\pi\to KK$ subprocess amplitude for the diagrams in Fig. 4 is written in the high-energy approximation as

$\dfrac{F_\pi^2(\hat{t})}{\hat{t}-m_\pi^2}\to\dfrac{i}{16\pi^2\hat{s}}\int d^2\kappa\dfrac{F_\pi^2(\hat{t}_1)}{\hat{t}_1-m_\pi^2}M^{K^*-\text{exch.}}_{\pi\pi\to K^+K^-}(\hat{t}_2),$

$\dfrac{F_\pi^2(\hat{u})}{\hat{u}-m_\pi^2}\to\dfrac{i}{16\pi^2\hat{s}}\int d^2\kappa\dfrac{F_\pi^2(\hat{u}_1)}{\hat{u}_1-m_\pi^2}M^{K^*-\text{exch.}}_{\pi\pi\to K^-K^+}(\hat{u}_2),$

$$(2.14)$$

with

$M^{K^*-\text{exch.}}_{\pi\pi\to K^+K^-}(\hat{t}_2)$

$= g_{\pi KK^*}F_{\pi KK^*}(\hat{t}_2)\dfrac{(p_3^{*\mu}+p_3^\mu)P_{\mu\nu}(p_4^{*\nu}+p_4^\nu)}{\hat{t}_2-m_{K^*}^2+im_{K^*}\Gamma_{K^*}}$

$\times g_{\pi KK^*}F_{\pi KK^*}(\hat{t}_2),$

$M^{K^*-\text{exch.}}_{\pi\pi\to K^-K^+}(\hat{u}_2)$

$= g_{\pi KK^*}F_{\pi KK^*}(\hat{u}_2)\dfrac{(p_3^{*\mu}+p_4^\mu)P_{\mu\nu}(p_4^{*\nu}+p_3^\nu)}{\hat{u}_2-m_{K^*}^2+im_{K^*}\Gamma_{K^*}}$

$\times g_{\pi KK^*}F_{\pi KK^*}(\hat{u}_2),$ $$(2.15)$$

where now $P_{\mu\nu}(k)=-g_{\mu\nu}+k_\mu k_\nu/m_{K^*}^2$ and we take $g_{\pi KK^*}=-\frac{1}{2}g_{\rho\pi\pi}$ [27].

The quantities $F(k^2)$ in Eqs. (2.13) and (2.15) describe couplings of extended $V=\rho,\omega,\phi$ and K^* mesons, respectively, and are parametrized in the exponential form:

$$F(k^2)=\exp\left(\frac{B_V}{4}(k^2-m_V^2)\right). \qquad (2.16)$$

Consistent with the definition of the coupling constant, the form factors are normalized to unity when the $V=\rho,\omega,\phi$ or K^* meson is on-mass-shell. We take $B_V=4\text{ GeV}^{-2}$.

The amplitudes given by formula (2.15) are corrected by the factors $(\hat{s}/\hat{s}_0)^{\alpha_{K^*}(k^2)-1}$ to reproduce the high-energy Regge dependence. We take the K^* meson trajectory as $\alpha_{K^*}(k^2)=0.25+\alpha'_{K^*}k^2$, with $\alpha'_{K^*}=0.83\text{ GeV}^{-2}$ [24].

The cross section is obtained by integration over the four-body phase space, which is reduced to eight dimensions and performed numerically:

$$\sigma=\int\frac{1}{2s}\overline{|\mathcal{M}|^2}(2\pi)^4\delta^4(p_a+p_b-p_1-p_2-p_3-p_4)$$

$$\times\frac{d^3p_1}{(2\pi)^32E_1}\frac{d^3p_2}{(2\pi)^32E_2}\frac{d^3p_3}{(2\pi)^32E_3}\frac{d^3p_4}{(2\pi)^32E_4}.$$

$$(2.17)$$

The details on how to conveniently reduce the number of kinematical integration variables are given, e.g., in [6].

III. OTHER DIFFRACTIVE PROCESSES

Up to now we have discussed only central diffractive contribution to the $pp\to ppK^+K^-$ reaction. In general, there are also contributions with other diffractive processes shown in Fig. 5, not evaluated so far in the literature. It is straightforward to evaluate the new diffractive contributions of diagrams (a)–(e) and the Born amplitudes are given below:

$$\mathcal{M}^{(a)}_{\lambda_a\lambda_b\to\lambda_1\lambda_2}=\bar{u}(p_1,\lambda_1)i\gamma_5 S_\Lambda(p_{1fl}^2)i\gamma_5 S_p(p_{1fp}^2)$$

$$\times u(p_a,\lambda_a)g_{\Lambda KN}^2 F_p^2(p_{1fp}^2)$$

$$\times F_\Lambda^2(p_{1fl}^2)isC_{IP}^{NN}\left(\frac{s}{s_0}\right)^{\alpha_{IP}(t_2)-1}$$

$$\times\exp\left(\frac{B_{IP}^{NN}t_2}{2}\right)\delta_{\lambda_2\lambda_b},$$ $$(3.1)$$
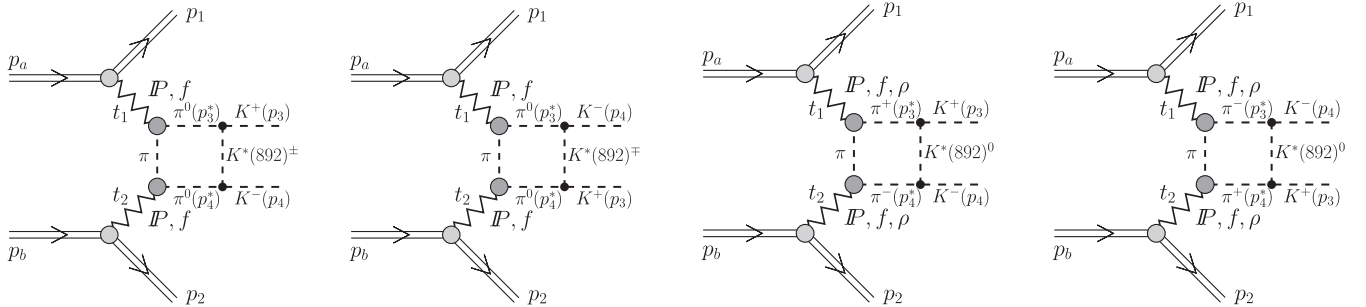
FIG. 4. The central diffractive mechanism of exclusive production of K^+K^- pairs via the $K^*(892)$ meson exchanges. f means a specific isoscalar meson.
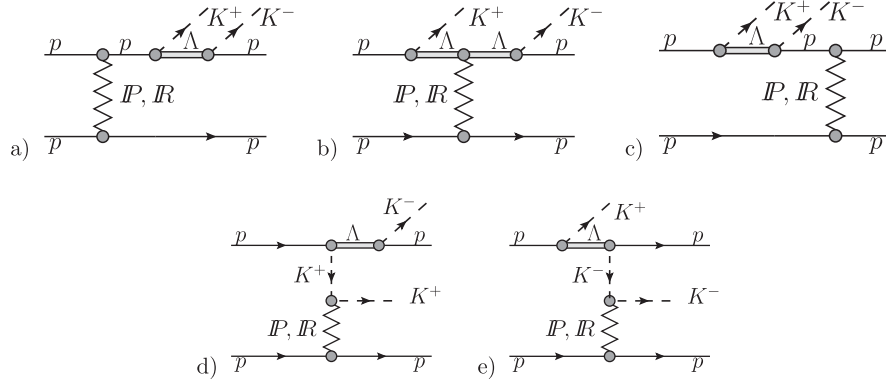
FIG. 5. Other diffractive contributions leading to the $pp \rightarrow ppK^+K^-$ channel.

$$
\begin{aligned}
\mathcal{M}^{(b)}_{\lambda_a \lambda_b \rightarrow \lambda_1 \lambda_2} = &\, \bar{u}(p_1, \lambda_1) i\gamma_5 S_\Lambda(p^2_{1fl}) \\
&\times S_\Lambda(p^2_{1il}) i\gamma_5 u(p_a, \lambda_a) g^2_{\Lambda KN} F^2_\Lambda(p^2_{1il}) \\
&\times F^2_\Lambda(p^2_{1fl}) i s_{124} C^{\Lambda N}_{I\!P} \left(\frac{s_{124}}{s_0}\right)^{\alpha_{I\!P}(t_2)-1} \\
&\times \left(\frac{s_{134}}{s^{pKK}_{th}}\right)^{\alpha_\Lambda(p^2_{1il})-1/2} \exp\left(\frac{B^{\Lambda N}_{I\!P} t_2}{2}\right) \delta_{\lambda_2 \lambda_b},
\end{aligned}
$$
(3.2)

$$
\begin{aligned}
\mathcal{M}^{(c)}_{\lambda_a \lambda_b \rightarrow \lambda_1 \lambda_2} = &\, \bar{u}(p_1, \lambda_1) S_p(p^2_{1ip}) i\gamma_5 S_\Lambda(p^2_{1il}) i\gamma_5 u(p_a, \lambda_a) \\
&\times g^2_{\Lambda KN} F^2_\Lambda(p^2_{1il}) F^2_p(p^2_{1il}) i s_{12} \\
&\times C^{NN}_{I\!P}\left(\frac{s_{12}}{s_0}\right)^{\alpha_{I\!P}(t_2)-1} \left(\frac{s_{14}}{s^{pK}_{th}}\right)^{\alpha_N(p^2_{1ip})-1/2} \\
&\times \left(\frac{s_{34}}{s^{KK}_{th}}\right)^{\alpha_\Lambda(p^2_{1il})-1/2} \exp\left(\frac{B^{NN}_{I\!P} t_2}{2}\right) \delta_{\lambda_2 \lambda_b},
\end{aligned}
$$
(3.3)

$$
\begin{aligned}
\mathcal{M}^{(d)}_{\lambda_a \lambda_b \rightarrow \lambda_1 \lambda_2} = &\, \bar{u}(p_1, \lambda_1) i\gamma_5 S_\Lambda(p^2_{1fl}) i\gamma_5 u(p_a, \lambda_a) \\
&\times S_K(p^2_{1fk}) g^2_{\Lambda KN} F^2_\Lambda(p^2_{1fl}) F^2_K(p^2_{1fk}) i s_{23} \\
&\times C^{KN}_{I\!P}\left(\frac{s_{23}}{s_0}\right)^{\alpha_{I\!P}(t_2)-1} \left(\frac{s_{134}}{s^{pKK}_{th}}\right)^{\alpha_K(p^2_{1fk})-1} \\
&\times \exp\left(\frac{B^{KN}_{I\!P} t_2}{2}\right) \delta_{\lambda_2 \lambda_b},
\end{aligned}
$$
(3.4)

$$
\begin{aligned}
\mathcal{M}^{(e)}_{\lambda_a \lambda_b \rightarrow \lambda_1 \lambda_2} = &\, \bar{u}(p_1, \lambda_1) i\gamma_5 S_\Lambda(p^2_{1il}) i\gamma_5 u(p_a, \lambda_a) \\
&\times S_K(p^2_{1ik}) g^2_{\Lambda KN} F^2_\Lambda(p^2_{1il}) F^2_K(p^2_{1ik}) i s_{24} \\
&\times C^{KN}_{I\!P}\left(\frac{s_{24}}{s_0}\right)^{\alpha_{I\!P}(t_2)-1} \left(\frac{s_{14}}{s^{pK}_{th}}\right)^{\alpha_K(p^2_{1ik})-1} \\
&\times \left(\frac{s_{13}}{s^{pK}_{th}}\right)^{\alpha_\Lambda(p^2_{1il})-1/2} \exp\left(\frac{B^{KN}_{I\!P} t_2}{2}\right) \delta_{\lambda_2 \lambda_b}, \quad (3.5)
\end{aligned}
$$

where $s_0 = 1 \text{ GeV}^2$ and $s^{pK}_{th} = (m_N + m_K)^2$, $s^{pKK}_{th} = (m_N + 2m_K)^2$. In the above equations $u(p_i, \lambda_i)$, $\bar{u}(p_f, \lambda_f) = u^\dagger(p_f, \lambda_f)\gamma^0$ are the Dirac spinors[normalized as $\bar{u}(p)u(p) = 2m_N$] of the initial and outgoing

protons with the four-momenta p and the helicities λ. Here $s_{ij} = (p_i + p_j)^2$, $s_{ijk} = (p_i + p_j + p_k)^2$ are squared invariant masses of the (i, j) and (i, j, k) systems. The four-momenta squared of the virtual particles are $p^2_{1il,2il} = (p_{a,b} - p_3)^2$, $p^2_{1fl,2fl} = (p_{1,2} + p_4)^2 = s_{14,24}$, $p^2_{1ik,2ik} = (p_{1il,2il} - p_{1,2})^2$, $p^2_{1fk,2fk} = (p_{a,b} - p_{1il,2il})^2$, $p^2_{1ip,2ip} = (p_{1il,2il} - p_4)^2$, $p^2_{1fp,2fp} = (p_{1fl,2fl} + p_3)^2 = s_{134,234}$. While the four-momenta squared of transferred kaons and protons are less than zero, it is not the case for transferred Λ's where $p^2_{1il,2il} < m^2_\Lambda$. The propagators for the intermediate particles are, respectively,

$$
S_K(k^2) = \frac{i}{k^2 - m^2_K}, \quad S_p(k^2) = \frac{i(k_\nu \gamma^\nu + m_N)}{k^2 - m^2_N},
$$

$$
S_\Lambda(k^2) = \frac{i(k_\nu \gamma^\nu + m_\Lambda)}{k^2 - m^2_\Lambda}.
$$
(3.6)

The form factors $F_i(k^2)$ correct for the off-shellness of the virtual particles and are parametrized as

$$
F_i(k^2) = \exp\left(\frac{-|k^2 - m^2_i|}{\Lambda^2_{\text{off}}}\right),
$$
(3.7)

where the parameter $\Lambda_{\text{off}} = 1$ GeV is taken in practical calculations. In our calculation, the ΛKN coupling constant is taken as $g^2_{\Lambda KN} = 14$ [28].

The Regge parameters in diagram (b) in Fig. 5 [see Eq. (3.2)] are not known precisely and are assumed to be $C^{\Lambda N}_{I\!P} \approx C^{NN}_{I\!P}$ (see Table I) and $B^{\Lambda N}_{I\!P} \approx B^{NN}_{I\!P} = 9 \text{ GeV}^{-2}$. To reproduce the high-energy Regge dependence, the amplitudes given in Eqs. (3.2), (3.3), (3.4), and (3.5) are corrected, e.g,. the amplitude of (3.4) is multiplied by a factor $(s_{134}/s^{pKK}_{th})^{\alpha_K(p^2_{1fk})-1}$. The parameters of the Regge trajectories used in the calculation are given as $\alpha_K(k^2) = 0.7(k^2 - m^2_K)$, $\alpha_p(k^2) = -0.3 + 0.9k^2$, $\alpha_\Lambda(k^2) = -0.6 + 0.9k^2$, for the kaon, proton, and Λ exchanges, respectively.

Finally, we consider the $\pi\pi \rightarrow KK$ rescattering mechanism shown in Fig. 6 which is particularly important rather at lower energies, e.g. for experiment PANDA to be built at GSI Darmstadt. We write the Born amplitude according to Feynman rules as
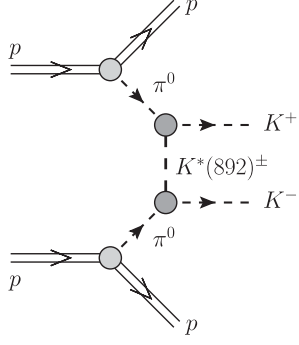
FIG. 6. The $\pi\pi \to KK$ subprocess leading to the $pp \to ppK^+K^-$ reaction.

$$\mathcal{M}^{\pi\pi-KK}_{\lambda_a\lambda_b \to \lambda_1\lambda_2}(\hat{t}, \hat{u})$$

$$= \bar{u}(p_1, \lambda_1)i\gamma_5 u(p_a, \lambda_a)$$

$$\times S_\pi(t_1)g_{\pi NN}F_{\pi NN}(t_1)F_{\pi K^*K}(t_1)(M^{K^*-\text{exch.}}_{\pi\pi \to K^+K^-}(\hat{t})$$

$$+ M^{K^*-\text{exch.}}_{\pi\pi \to K^-K^+}(\hat{u}))\bar{u}(p_2, \lambda_2)i\gamma_5 u(p_b, \lambda_b)$$

$$\times S_\pi(t_2)g_{\pi NN}F_{\pi NN}(t_2)F_{\pi K^*K}(t_2), \qquad (3.8)$$

where $g^2_{\pi NN}/4\pi = 13.5$ value is taken and the $M^{K^*-\text{exch.}}_{\pi\pi \to KK}$ amplitudes are given by Eq. (2.15).

IV. RESULTS

Now we wish to show results and predictions for existing and future experiments. We start with the DPE mechanism, which dominates at midrapidities. In Fig. 7, we show the two-kaon invariant mass distribution at the center-of-mass energy of the CERN ISR $\sqrt{s} = 62$ GeV [12]. In this calculation, the experimental cuts on the rapidity of both kaons and on longitudinal momentum fractions (Feynman-x, $x_F = 2p_\parallel/\sqrt{s}$) of both outgoing protons are

included. The experimental data show some small peaks above our flat model continuum. They correspond to the K^+K^- resonances [e.g. $f_2(1270)$, $f'_2(1525)$] which are not included explicitly in our calculation. In the present analysis, we are interested mostly what happens above the region $M_{KK} > 2$–3 GeV (see the right panel). The results depend on the value of the nonperturbative, *a priori* unknown parameter of the form factor responsible for off-shell effects [see Eq. (2.8)]. Our model with the $\Lambda^2_{\text{off}} = 2$ GeV^2 cutoff parameter fitted to the data provides an educated extrapolation to the unmeasured region. We compare results without (dotted lines) and with absorption corrections including the KK-rescattering effect (solid line). At the χ_{c0} mass the KK rescattering leads to an enhancement of the cross section compared to the calculation without KK rescattering. Below, we shall use also these background predictions when analyzing the signal (χ_{c0}) to the background ratio.

In Fig. 8 we show differential distributions for the $pp \to ppK^+K^-$ reaction at $\sqrt{s} = 7$ TeV without (dotted line) and with (solid line) the absorptive corrections. In most distributions the shape is almost unchanged. The only exception is the distribution in proton transverse momentum where we predict a damping of the cross section at a small proton p_t and an enhancement of the cross section at a large proton p_t. This effect is caused by multiple proton scattering (double scattering in our model). Such an effect is well known, e.g., in elastic proton-proton scattering where multiple scattering leads to the appearance of dips and maxima of the t dependence of the cross section observed in experimental distributions. In the literature, for simplicity, often three- or four-body cross sections are multiplied by an average gap survival factor which leads to a uniform damping of the cross section. This is not a sufficient approximation for some observables as discussed here.
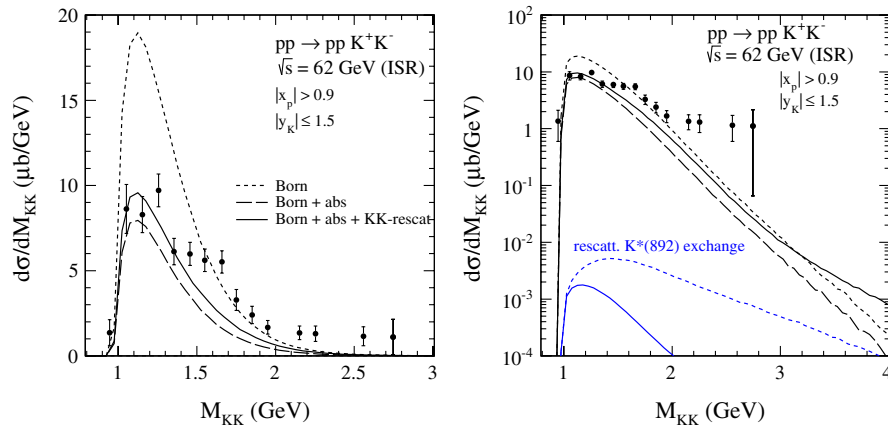
FIG. 7 (color online). Differential cross section $d\sigma/dM_{KK}$ for the $pp \to ppK^+K^-$ reaction at $\sqrt{s} = 62$ GeV with experimental cuts relevant for the CERN ISR experimental data from Ref. [12]. The right panel shows the same in the logarithmic scale. Results without (dotted line) and with (solid line) absorption effects are shown. Here $\Lambda^2_{\text{off}} = 2$ GeV^2 and $\Lambda_{\text{int}} = 2$ GeV. In the right panel the central diffractive mechanism with $K^*(892)$ meson exchanges corresponding to diagrams in Fig. 4 without (dashed line) and with (solid line) a K^* Reggezaition are shown in addition.
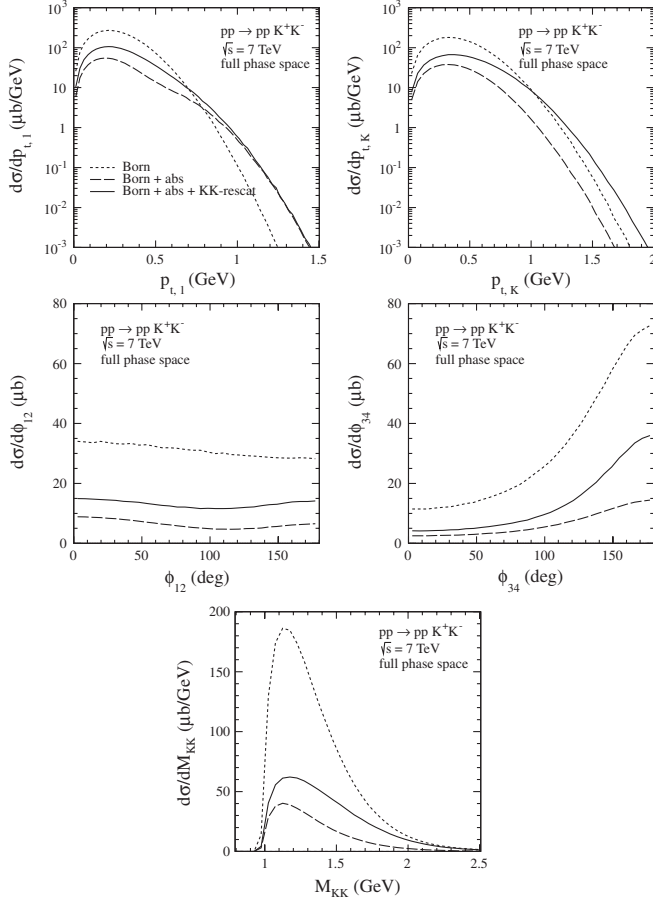
FIG. 8. Differential cross sections for the $pp \to ppK^+K^-$ reaction at $\sqrt{s} = 7$ TeV without (dotted line) and with (solid line) the absorption effects. These calculations were done with the cutoff parameter $\Lambda_{\text{off}}^2 = 2$ GeV^2 and $\Lambda_{\text{int}} = 2$ GeV.

In Fig. 9 we show differential distributions in kaon rapidity $y_K = y_3 = y_4$ for the $pp \to ppK^+K^-$ reaction at $\sqrt{s} = 0.5, 1.96, 7$ TeV without (upper lines) and with (bottom lines) absorption effects. The integrated cross section slowly rises with incident energy. The reader is asked to notice that the energy dependence of the cross section at $y_K \approx 0$ is reversed by the absorption effects
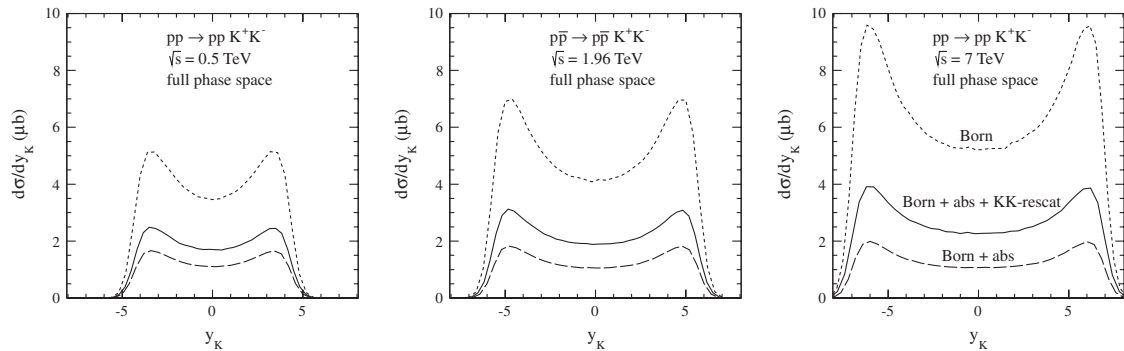
which are stronger at higher energies. In our calculation, we include both Pomeron and Reggeon exchanges. The camel-like shape of the distributions is due to the interference of the components in the amplitude. In Fig. 10 we show the distribution in y_K (y_3 or y_4) for all ingredients included (thick solid line), when only Pomeron-Pomeron contribution is included (solid line), and for Pomeron-Reggeon (Reggeon-Pomeron) contributions separated (grey lines that peak at forward or backward hemispheres).

In Fig. 11 we show distributions in the two-dimensional (y_3, y_4) space at $\sqrt{s} = 0.5, 1.96, 7$ TeV for the central diffractive contribution. The cross section grows with $\sqrt{s}$. At high energies the kaons are emitted preferentially in the same hemispheres, i.e., $y_3, y_4 > 0$ or $y_3, y_4 < 0$. In this calculation the cutoff parameter $\Lambda_{\text{off}}^2 = 2$ GeV^2.

In Fig. 12 we show distributions in the ($p_{t,K}, M_{KK}$) space at $\sqrt{s} = 0.5, 7$ TeV for the central diffractive contribution. As expected, we observe strong correlation between the two variables.

Now we wish to compare differential distributions of kaon from the χ_{c0} decay with those for the continuum kaons. The amplitude for exclusive central diffractive χ_{c0} meson production was calculated within the k_t factorization approach including virtualities of active gluons [13] and the corresponding cross section is calculated with the help of unintegrated gluon distribution functions (UGDFs) known from the literature. We apply the following simple procedure. First, we calculate the two-dimensional distribution $d\sigma(y, p_t)/dy dp_t$, where y is rapidity and p_t is the transverse momentum of χ_{c0}. The decay of $\chi_{c0} \to K^+K^-$ is included then in a simple Monte Carlo program assuming isotropic decay of the scalar χ_{c0} meson in its rest frame. The kinematical variables of kaons are transformed to the overall center-of-mass frame where extra cuts are imposed. Including the simple cuts allows us to construct several differential distributions in different kinematical variables.

In Fig. 13 we show a two-kaon invariant mass distribution for the central diffractive KK continuum and the contribution from the decay of the χ_{c0} meson (see

FIG. 9. Differential cross section $d\sigma/dy_K$ for the $pp \to ppK^+K^-$ reaction at $\sqrt{s} = 0.5, 1.96, 7$ TeV with $\Lambda_{\text{off}}^2 = 2$ GeV^2. The results without (upper lines) and with (bottom lines) absorption effects due to the pp interaction and KK-rescattering are shown too.
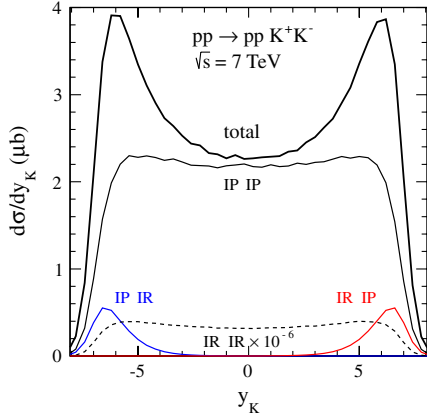
FIG. 10 (color online). Differential cross section $d\sigma/dy_K$ for the $pp \to ppK^+K^-$ reaction at $\sqrt{s} = 7$ TeV with $\Lambda^2_{\rm off} = 2$ GeV^2. The different lines corresponds to the situation when all and only some components in the amplitude are included. The details are explained in the main text.

the peak at $M_{KK} \simeq 3.4$ GeV) and the contribution from the decay of the ϕ meson. The cross section for exclusive production of the ϕ meson has been calculated within a pQCD k_t-factorization approach in Ref. [29]. In these

figures, the resonant $\mathcal{R} = \phi, \chi_{c0}$ distributions were parametrized in the Breit-Wigner form:

$$\frac{d\sigma}{dM_{KK}} = \mathcal{B}(\mathcal{R}$$

$$\to K^+K^-)\sigma_{pp \to pp\mathcal{R}} 2M_{KK} \frac{1}{\pi}$$

$$\times \frac{M_{KK}\Gamma_{\mathcal{R}}}{(M^2_{KK} - m^2_{\mathcal{R}})^2 + M^2_{KK}\Gamma^2_{\mathcal{R}}}, \quad (4.1)$$

with parameters according to the Particle Data Group in Ref. [20]. In the calculation of the χ_{c0} distributions, we use GRV94 next-to-leading order (NLO) [30] and GJR08 NLO [31] collinear gluon distributions. The cross sections for the ϕ and χ_{c0} production and for the background include absorption effects. While the upper row shows the cross section integrated over the full phase space at different energies, the lower rows show results including the relevant kaon pseudorapidity restrictions $-1 < \eta_{K^+}, \eta_{K^-} < 1$ (RHIC and Tevatron) and $-2.5 < \eta_{K^+}, \eta_{K^-} < 2.5$ (LHC). Shown are only purely theoretical predictions. In reality, the situation is, however, somewhat worse as both protons and, in particular, kaon pairs are measured with a certain
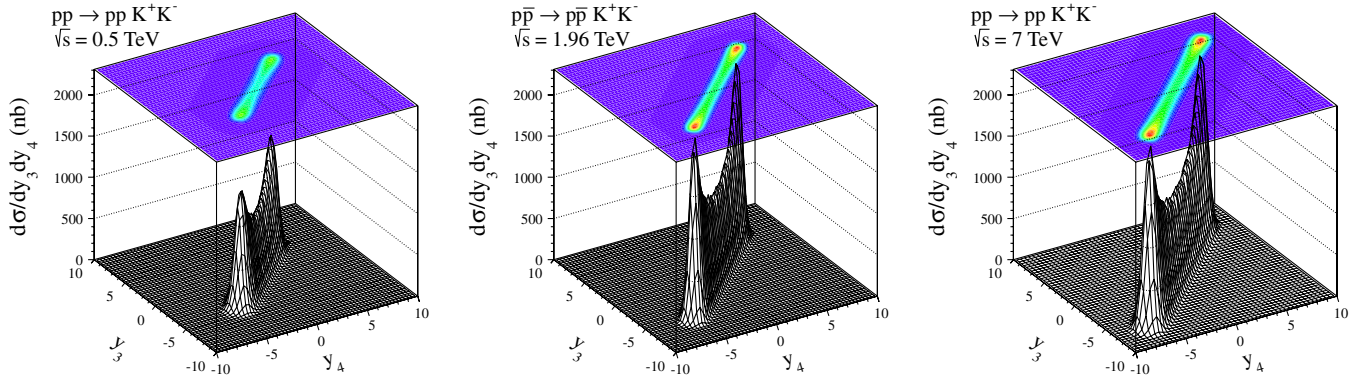
FIG. 11 (color online). Differential cross section in (y_3, y_4) for the central diffractive contribution for three incident energies $\sqrt{s} = 0.5, 1.96, 7$ TeV. We show a standard lego plot as well as a map with standard map color coding above the lego plot. The absorption effects were included here.
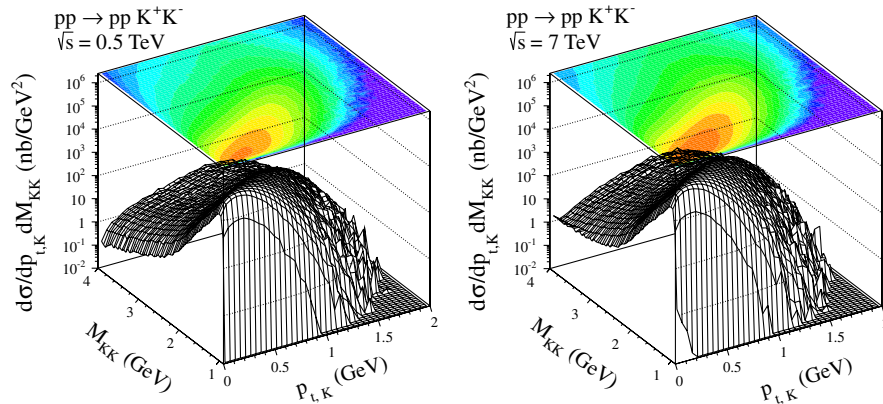
FIG. 12 (color online). Differential cross section in $(p_{t,K}, M_{KK})$ for the central diffractive contribution for two incident energies $\sqrt{s} = 0.5, 7$ TeV. The absorption effects were included here.
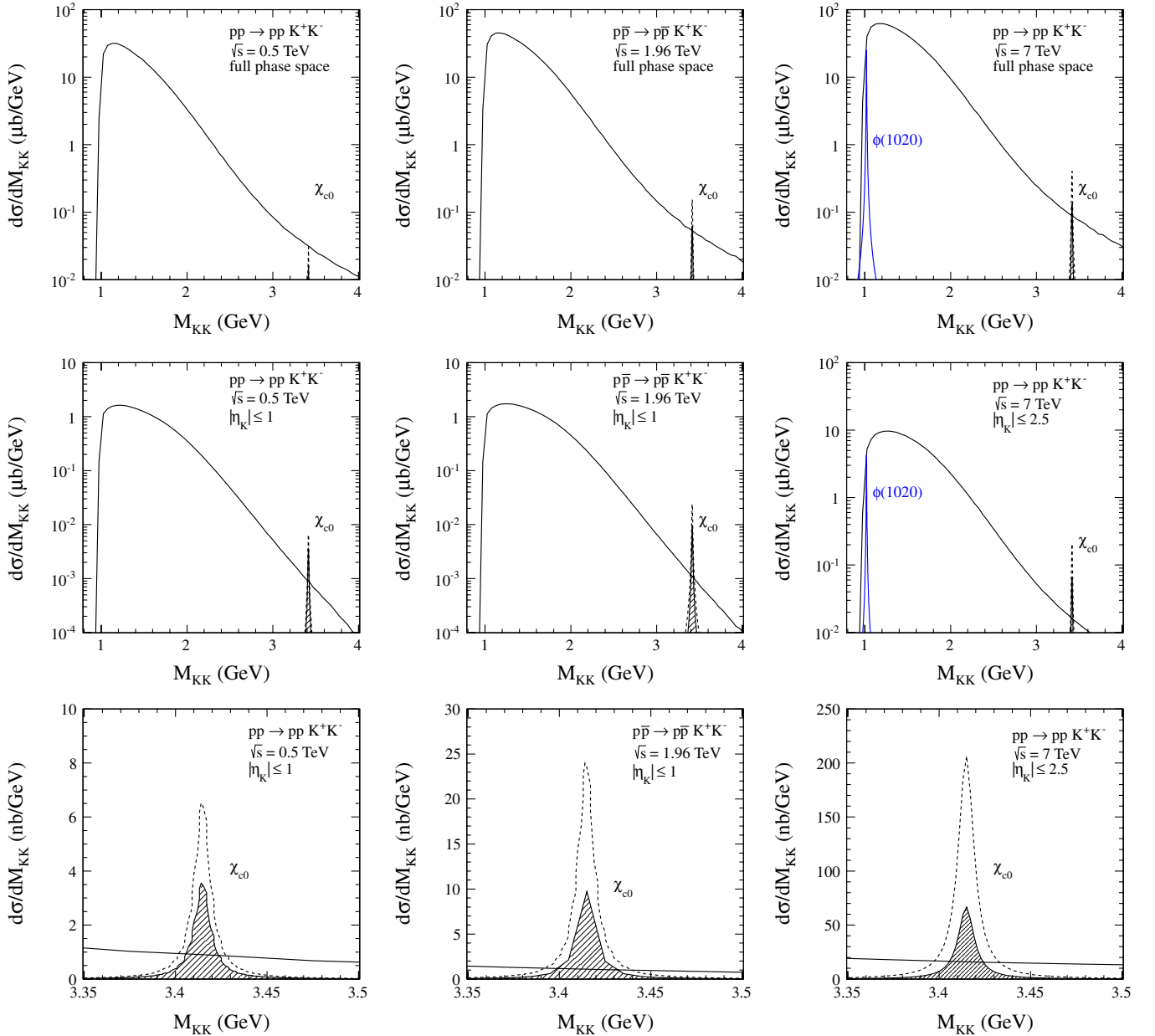
FIG. 13 (color online). The K^+K^- invariant mass distribution at $\sqrt{s} = 0.5, 1.96, 7$ TeV integrated over the full phase space (upper row) and with the detector limitations in kaon pseudorapidities (lower rows). The solid lines present the KK continuum with the cutoff parameters $\Lambda_{off}^2 = 2$ GeV^2. The χ_{c0} contribution is calculated with the GRV94 NLO (dotted lines) and GJR08 NLO (filled areas) collinear gluon distributions. The cross section for ϕ contribution at $\sqrt{s} = 7$ TeV is calculated as in [29]. The absorption effects were included in the calculations. A clear χ_{c0} signal with a relatively small background can be observed.

precision which leads to an extra smearing in M_{KK}. While the smearing is negligible for the background, it leads to a modification of the Breit-Wigner peak for the χ_{c0} meson.[1] The results with more modern Glück-Jimenez-Delgado-Reya (GJR) UGDF are smaller by about a factor of 2–3

than those for somewhat older Glück-Reya-Vogt (GRV) UGDF.

In Fig. 14 we show distributions in kaon transverse momenta. The kaons from the χ_{c0} decay are placed at slightly larger $p_{t,K}$. This can therefore be used to get rid of the bulk of the continuum by imposing an extra cut on the kaon transverse momenta. It is not the case for the kaons from the ϕ decay which are placed at lower $p_{t,K}$.

In Table II we have collected numerical values of the integrated cross sections for exclusive production of

---

[1]An additional experimental resolution not included here can be taken into account by an extra convolution of the Breit-Wigner shape with an additional Gaussian function.
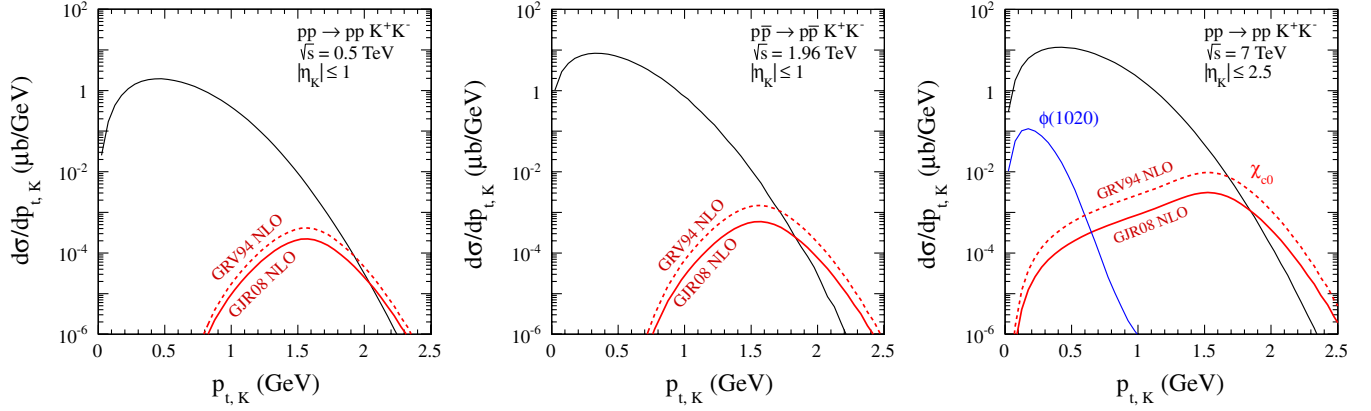
FIG. 14 (color online).   Differential cross section $d\sigma/dp_{t,K}$ at $\sqrt{s} = 0.5, 1.96, 7$ TeV with cuts on the kaon pseudorapidities. The diffractive background was calculated with the cutoff parameter $\Lambda^2_{\text{off}} = 2$ GeV^2. Results for the kaons from the decay of the χ_{c0} meson including the K^+K^- branching ratio, for the GRV94 NLO (upper lines) and GJR08 NLO (bottom lines) UGDFs, are shown. In the right panel ϕ meson contribution is shown in addition. The absorption effects were included here.

K^+K^- at different energies. In Table III we have collected in addition numerical values of the integrated cross sections [see $\sigma_{pp \to pp\chi_{c0}}$ in Eq. (4.1)] for exclusive χ_{c0} production for some selected UGDFs at different energies.

In Fig. 15 we present rapidity distribution of K^+ (left panel) and rapidity distribution of K^- (right panel) including only diagrams shown in Fig. 5. The contribution for individual diagrams (a)–(e) are also shown. In the discussion here, in the new mechanism, not only protons but also kaons are produced dominantly in very forward or

TABLE II.   Integrated cross sections in μb (with absorption corrections) for exclusive K^+K^- production at different energies. In this calculations we have taken into account the relevant limitations in the kaon pseudorapidities $|\eta_K| < 1$ at RHIC and Tevatron, $|\eta_K| < 2.5$ at LHC.

$\sqrt{s}$ (TeV)	Full phase space	With cuts on η_K
0.5	18.47	1.21
1.96	27.96	1.37
7	41.14	7.38

very backward directions. The two kaons have, however, similar rapidities, which means that there is no gap between kaons. This means that both kaons are preferentially produced very forward or very backward, forming a large size gap between kaons and one of the protons (backward or forward, respectively). Please note a very limited range of rapidities shown in the figure. The Reggezation leads to an extra damping of the cross section. The cross section is much smaller than that for the DPE mechanism discussed above. It is particularly interesting that the distributions for K^+ and K^- have slightly different shapes.

Finally, the general situation at high energies is sketched in Fig. 16. In the discussion in this paper, the central diffractive (DD) contribution lays along the diagonal $y_3 = y_4$ and the classical DPE is placed in the center $y_3 \approx y_4$. While the contribution from the diagrams in Fig. 5 is predicted at $y_3, y_4 \sim y_{\text{beam}}$ or $y_3, y_4 \sim y_{\text{target}}$, the $\pi\pi \to KK$ contribution (see Fig. 6) is predicted at ($y_3 \sim y_{\text{beam}}$ and $y_4 \sim y_{\text{target}}$) or ($y_3 \sim y_{\text{target}}$ and $y_4 \sim y_{\text{beam}}$), i.e., well separated from the central diffractive contribution. The separation in the (y_3, y_4) space can be used to separate the two contributions experimentally.

TABLE III.   Integrated cross sections in nb (with absorption corrections) for exclusive χ_{c0} production at different energies with the GRV94 NLO and GJR08 NLO collinear gluon distributions. In these calculations we have taken into account the relevant limitations in the kaon pseudorapidities $|\eta_K| < 1$ at RHIC and Tevatron, $|\eta_K| < 2.5$ at LHC, and the lower cut on both kaon transverse momenta $|p_{t,K}| > 1.5$ GeV.

$\sqrt{s}$ (TeV)	full phase space		with cuts on η_K		with cuts on η_K and $p_{t,K}$	
	GRV	GJR	GRV	GJR	GRV	GJR
0.5	82.9	44.0	17.3	9.4	5.7	3.1
1.96	406.3	165.1	63.7	25.9	20.7	8.3
7	1076.7	347.7	548.6	177.1	114.5	36.6
14	1566.3	449.2	735.0	210.9	152.1	43.1
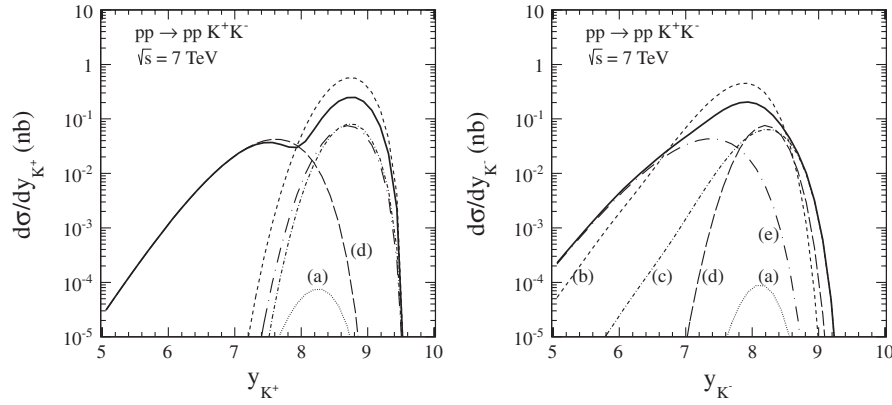
FIG. 15. Differential cross sections $d\sigma/dy_{K^+}$ (left panel) and $d\sigma/dy_{K^-}$ (right panel) for the $pp \rightarrow ppK^+K^-$ reaction at $\sqrt{s} = 7$ TeV. The solid line represents the coherent sum of all amplitudes. The dotted, dashed, dash-dotted, long-dashed, long-dash-dotted lines correspond to contributions from diagrams (a)–(e) in Fig. 5. The Reggeization of the particle exchange was included here.
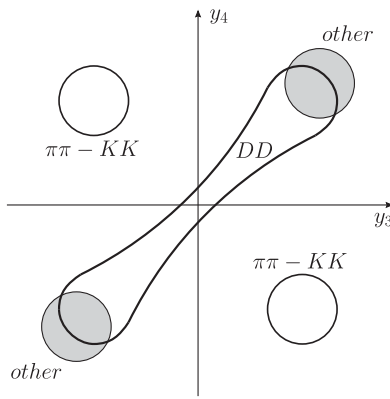
FIG. 16. A schematic localization of different mechanisms for the $pp \rightarrow ppK^+K^-$ reaction at high energies.

V. CONCLUSIONS

In the present paper, we have calculated several differential observables for the exclusive $pp \rightarrow ppK^+K^-$ and $p\bar{p} \rightarrow p\bar{p}K^+K^-$ reactions. The full amplitude of the central diffractive process was calculated in a simple model with parameters adjusted to low energy data. The energy dependence of the amplitudes of the KN subsystems was parametrized in the Regge form, which describes the total and elastic cross section for the KN scattering. This parametrization includes both the leading Pomeron trajectory as well as the subleading Reggeon exchanges. We have predicted large cross sections for RHIC, Tevatron, and LHC which allows us to hope that the distributions presented by us will be measured.

We have also calculated the contributions of several diagrams where kaons are emitted from the proton lines. These mechanisms contribute at forward and backward regions and do not disturb the observation of the central DPE component.

At the Tevatron, the measurement of exclusive production of χ_c via decay in the $J/\psi + \gamma$ channel cannot provide production cross sections for different species of χ_c. In this decay channel, the contributions of χ_c mesons with different spins are similar and experimental resolution is not sufficient to distinguish them. At the LHC, the situation should be better.

In the present paper, we have analyzed a possibility to measure the exclusive production of the χ_{c0} meson in the proton-(anti)proton collisions at the LHC, Tevatron, and RHIC via the $\chi_{c0} \rightarrow K^+K^-$ decay channel. We have performed detailed studies of several differential distributions and demonstrated how to impose extra cuts in order to improve the signal-to-background ratio. We have shown that relevant measurements at RHIC, Tevatron and LHC are possible. Since the cross section for exclusive χ_{c0} production is much larger than for $\chi_{c(1,2)}$ and the branching fraction to the KK channel for χ_{c0} is larger than that for χ_{c2} (χ_{c1} does not decay into two kaons) the two-kaon channel should provide useful information about the χ_{c0} exclusive production.

[1] A. Dzyuba *et al.*, Phys. Lett. B **668**, 315 (2008).
[2] Ju-Jun Xie and Colin Wilkin, Phys. Rev. C **82**, 025210 (2010).
[3] M. G. Albrow, T. D. Coughlin, and J. R. Forshaw, Prog. Part. Nucl. Phys. **65**, 149 (2010).
[4] A. Szczurek and P. Lebiedowicz, Nucl. Phys. **A826**, 101 (2009).
[5] P. Lebiedowicz, A. Szczurek, and R. Kamiński, Phys. Lett. B **680**, 459 (2009).
[6] P. Lebiedowicz and A. Szczurek, Phys. Rev. D **81**, 036003 (2010).
[7] P. Lebiedowicz and A. Szczurek, Phys. Rev. D **83**, 076002 (2011).
[8] R. Staszewski, P. Lebiedowicz, M. Trzebiński, J. Chwastowski, and A. Szczurek, Acta Phys. Polon. B **42**, 1861 (2011).
[9] T. A. Armstrong *et al.* (WA76 Collaboration), Z. Phys. C **51**, 351 (1991).
[10] D. Barberis *et al.* (WA102 Collaboration), Phys. Lett. B **462**, 462 (1999).
[11] T. Akesson *et al.* (AFS Collaboration), Nucl. Phys. **B264**, 154 (1986).
[12] A. Breakstone *et al.* (ABCDHW Collaboration), Z. Phys. C **42**, 387 (1989).
[13] R. S. Pasechnik, A. Szczurek, and O. V. Teryaev, Phys. Rev. D **78**, 014007 (2008).
[14] R. S. Pasechnik, A. Szczurek, and O. V. Teryaev, Phys. Lett. B **680**, 62 (2009).
[15] R. S. Pasechnik, A. Szczurek, and O. V. Teryaev, Phys. Rev. D **81**, 034024 (2010).
[16] L. A. Harland-Lang, V. A. Khoze, M. G. Ryskin, and W. J. Stirling, Eur. Phys. J. C **65**, 433 (2010).
[17] L. A. Harland-Lang, V. A. Khoze, M. G. Ryskin, and W. J. Stirling, Eur. Phys. J. C **71**, 1545 (2011).
[18] C. Amsler and F. E. Close, Phys. Rev. D **53**, 295 (1996).
[19] T. Aaltonen *et al.* (CDF Collaboration), Phys. Rev. Lett. **102**, 242001 (2009).
[20] K. Nakamura *et al.* (Particle Data Group), J. Phys. G **37**, 075021 (2010).
[21] P. Lebiedowicz, R. Pasechnik, and A. Szczurek, Phys. Lett. B **701**, 434 (2011).
[22] M. Ablikim *et al.* (BESIII Collaboration), Phys. Rev. D **83**, 112009 (2011).
[23] A. Donnachie and P. V. Landshoff, Phys. Lett. B **296**, 227 (1992).
[24] M. Guidal, J. M. Laget, and M. Vanderhaeghen, Nucl. Phys. **A627**, 645 (1997); Byung Geel Yu, Tae Keun Choi, and W. Kim, Phys. Rev. C **83**, 025208 (2011).
[25] A. Szczurek, N. N. Nikolaev, and J. Speth, Phys. Rev. C **66**, 055206 (2002).
[26] A. Szczurek and J. Speth, Nucl. Phys. **A728**, 182 (2003).
[27] O. Krehl, R. Rapp, and J. Speth, Phys. Lett. B **390**, 23 (1997).
[28] J. M. Laget, Phys. Lett. B **259**, 24 (1991).
[29] A. Cisek, W. Schäfer, and A. Szczurek, Phys. Lett. B **690**, 168 (2010).
[30] M. Glück, E. Reya, and A. Vogt, Z. Phys. C **67**, 433 (1995).
[31] M. Glück, D. Jimenez-Delgado, and E. Reya, Eur. Phys. J. C **53**, 355 (2008); M. Glück, D. Jimenez-Delgado, E. Reya, and C. Schuck, Phys. Lett. B **664**, 133 (2008).
[32] A. Eide *et al.*, Nucl. Phys. **B60**, 173 (1973); I. Ambats *et al.*, Phys. Rev. D **9**, 1179 (1974); C. W. Akerlof *et al.*, Phys. Rev. D **14**, 2864 (1976); D. S. Ayres *et al.*, Phys. Rev. D **15**, 3105 (1977).